High thermoelectric performance in $Bi_{2-x}Pb_xBa_2Co_2O_x$ promoted by directional growth and annealing

M. A. Madre[1], F. M. Costa[2], N. M. Ferreira[2], S. I. R. Costa[3], Sh. Rasekh[1], M. A. Torres[1], J. C. Diez[1], V. S. Amaral[2,3], J. S. Amaral[2,3], A. Sotelo[1,*]

[1]Instituto de Ciencia de Materiales de Aragón, ICMA (CSIC-Universidad de Zaragoza), Mª de Luna, 3. 50018 Zaragoza, Spain.

[2]i3N, Departamento de Física, Universidade de Aveiro, 3810-193 Aveiro, Portugal

[3]CICECO, Materials and Ceramic Eng. Dept., University of Aveiro, 3810-193 Aveiro (Portugal)

Abstract

$Bi_{2-x}Pb_xBa_2Co_2O_y$ (x=0.0, 0.2, 0.4, and 0.6) misfit compounds were grown by the laser floating zone technique. Microstructural analysis has shown the formation of thermoelectric grains together with high amount of secondary phases. Thermoelectric grains orientation is increased until 0.4Pb, while further substitution drastically destroys the preferential grain orientation. Electrical resistivity is very low compared with the values obtained in sintered materials, spectacularly increasing power factor. Moreover, the performance of these materials was further improved subjecting the as-grown samples to a postannealing step due to the rise of thermoelectric phase content. These microstructural modifications led to a high decrease of electrical resistivity, improving power factor in around a factor two at room temperature, compared with the as-grown samples. Moreover, the low thermal conductivity of the textured annealed samples leads to a maximum estimated ZT value of 0.53 for the 0.2 Pb-doped samples, much higher than the reported in literature.

Keywords: Ceramics; Doping; Grain growth; Electrical properties; Thermopower

Corresponding author: Andres Sotelo
e-mail: asotelo@unizar.es
Address: C/Maria de Luna, 3. 50018-Zaragoza (Spain)
Tel: +34 976762617

Fax: +34 976761957

1. Introduction

Nowadays, there is a great and growing interest in the development of new and clean energy sources in order to fight against global warming. These green energy sources should decrease the release of greenhouse gases, as CO_2, produced in the classical energy transforming systems. On the other hand, it is still difficult to avoid the use of fossil fuels in many applications, as in automobiles or electrical power production, with a relatively low efficiency (~ 40 %) [1]. In this scenario, thermoelectric (TE) energy conversion, based on the well-known Seebeck effect, can be used to transform solar energy into electricity at lower cost than photovoltaic energy [2]. Moreover, it has shown important advantages (for example, they are silent and have non moving parts) to be applied in harvesting waste heat in these classical energy transforming systems [3]. The efficiency characterization of these TE materials is performed through the dimensionless figure of merit, ZT, which is calculated as $T\ S^2\ \rho^{-1}\ \kappa^{-1}$, where T, S, ρ, and κ are the absolute temperature, Seebeck coefficient, electrical resistivity and thermal conductivity, respectively [4]. As a consequence, a high performance TE material should have low thermal conductivity, high power factor ($PF = S^2\ \rho^{-1}$), and high working temperatures.

At present, some practical applications of TE devices can be found in vehicles exhausts and in cooling systems. These TE devices are formed by different intermetallic or semiconducting materials, as Bi-Te-based ones, with high associated costs, and relatively low working temperatures. Moreover, most of these materials are composed of scarce, heavy, and/or toxic elements which are not environmental friendly. Nevertheless, since the discovery in 1997 of good TE properties in Na_xCoO_2 [5], many studies have been performed in transition metal oxide (TMO's) based materials. These materials, such as $Bi_2Ca_2Co_2O_x$ [6,7], $Bi_2Sr_2Co_2O_x$ [8,9], $Bi_2Ba_2Co_2O_x$ [10], or $Ca_3Co_4O_9$ [11,12], are based in cheaper, more abundant and environmentally friendly, and chemically stable at high temperatures under air. All these characteristics have greatly increased the interest in these TMO's-based materials.

Crystallographic studies of these materials have shown that they can be described by a monoclinic structure formed by two different sublattices which are alternately stacked [13]. One is the CoO_2 conductive layer with CdI_2-type

structure, while the other one is an insulating rock-salt-type. Both sublattices possess the same lattice parameters, except in the b-axis length, leading to a misfit along this direction [14]. As it is well-known, these materials show a very important crystallographic anisotropy which is reflected in a high electrical conductivity one. As a consequence, the alignment of grains along their conducting planes can be used to drastically reduce the electrical resistivity in the bulk materials. This process would allow enhancing ZT to values close to the obtained in single crystals. Many techniques have been used to produce such grain alignment, as hot-pressing [15], spark plasma sintering (SPS) [16], laser floating zone (LFZ) [17], or the electrically assisted laser floating zone [18], which have shown their ability to improve TE performance of bulk materials by the alignment of grains.

On the other hand, doping processes have been also shown that TE properties can be tuned up by using the adequate dopants and proportions, as it is the case of different metals for Ca substitution in $Ca_3Co_4O_9$ [19], or Pb for Bi in $Bi_2Sr_2Co_{1.8}O_x$ [20]. Moreover, the synthesis techniques can also drastically modify the grain sizes and their connectivity, leading to improved properties in the final bulk materials [21].

Taking into account the above considerations, the aim of the present work is studying the effect of relatively low Pb substitutions for Bi in the $Bi_2Ba_2Co_2O_x$ thermoelectric material. Pb has been selected as dopant due to its unique properties which make it essential in many compounds and applications, as for example in PZT piezoelectrics [22], or as dopant, stabilizing the High-Tc Bi-2223 superconducting phase [23]. It has been prepared by a polymer solution method developed in our laboratory [24], followed by texturing using the laser floating zone melting technique [17]. Moreover, as it was determined in previous works in similar systems, the as grown materials possess a high amount of secondary phases [25]. As a consequence, some samples were annealed to increase the amount of the thermoelectric phase. The thermoelectric properties of these $Bi_{2-x}Pb_xBa_2Co_2O_y$ textured ceramics (with x=0, 0.2, 0.4, and 0.6), before and after annealing, have been determined and correlated with their structure and microstructure.

2. Experimental

The $Bi_{2-x}Pb_xBa_2Co_2O_y$ ceramics (with x=0, 0.2, 0.4, and 0.6) were prepared from $Bi(CH_3CO_2)_3$ (99.99 + %, Aldrich), $Pb(CH_3CO_2)_2 \cdot 3H_2O$ (≥ 99%, Aldrich), $Ba(CH_3CO_2)_2$ (≥ 99%, Aldrich), and $Co(CH_3CO_2)_2 \cdot 4H_2O$ (98%, Panreac) commercial powders. They were weighed in the appropriate proportions and dissolved in a mixture of distilled H_2O and glacial acetic acid (ACS Reagent, Panreac). To the clear pink solution, Polyethylenimine (PEI) (50% aqueous, Aldrich) was added to the above solution which turned darker immediately due to the nitrogen-metal bond formation. Partial evaporation of water and acetic acid has been performed in a rotary evaporator until a final volume of around 20 % of the initial one. The concentrated solution was then placed onto a hot plate for further solvent evaporation until a very dark pink paste appeared. Further heating turn this paste to violet colour, followed by a slow autocombustion with the release of brown fumes (nitrogen oxides). The mixture was manually milled and thermally treated at 700 and 750ºC for 12 h, with an intermediate milling, following the procedure described elsewhere [26] to decompose the alkaline earth carbonates. This decomposition step is very important to produce well aligned grains by the laser floating zone, due to the fact that the remaining carbonates would decompose during the texturing process inside the molten zone. As a consequence, the melt would be disturbed by the CO_2 bubbles produced in the decomposition process, leading to the growth front destabilization and producing grains misalignments.

The final powder was then isostatically pressed under 200 MPa during one minute to produce cylindrical green ceramics (2-3 mm diameter). These cylinders were used as feed in a LFZ device equipped with a continuous power Nd:YAG laser (λ = 1064 nm), following the experimental procedure described elsewhere [27]. All the LFZ-grown samples were processed at 30 mm h^{-1} under air with a seed rotation of 3 rpm to maintain the cylindrical geometry. Moreover, the feed was rotated at 15 rpm in the opposite direction, in order to ensure compositional homogeneity of the molten zone. After the texturing process, long (> 150 mm) and geometrically homogeneous textured cylindrical rods of around 2 mm diameter were produced. The textured bars were cut into suitably sized pieces for their TE characterization (~ 15 mm long). As mentioned previously, as-grown materials are characterized by a relatively high amount of secondary

phases. As a consequence, some of the samples were annealed at 700 ºC for 24 h, in air atmosphere, to increase the proportion of the thermoelectric phase in the samples.

The identification of the main phases in the textured samples was performed by powder X-ray diffraction (XRD) utilizing a Rigaku D/max-B X-ray powder diffractometer (CuKα radiation) with 2θ ranging between 10 and 70 degrees. In order to determine the adequate temperature for annealing the as-grown samples, DTA analyses were performed in a TA Instrument (SDT Q600) system between room temperature and 800 ºC.

Microstructural observations were performed on polished as-grown and annealed samples using backscattered electrons in a Zeiss Merlin field emission scanning electron microscope (FESEM) equipped with an energy dispersive spectrometry (EDS) analysis system. Micrographs of these samples have been recorded to analyze the different phases and their distribution.

Steady-state simultaneous measurements of resistivity and Seebeck coefficient were determined by the standard dc four-probe technique in a LSR-3 apparatus (Linseis GmbH) between 50 and 650 ºC under He atmosphere, with an estimated error of 4 % in each parameter. From these data, samples performances were determined using PF values.

Finally, thermal conductivity was determined at room temperature in the annealed samples using the transient plane source technique (Hot Disk TPS 2500 s), which possess an accuracy better than 5 %, as indicated by the system manufacturer. This method uses an electrically conducting pattern element acting both as a temperature sensor and heat source, insulated with two thin layers of Kapton (70 μm). The TPS element is assembled between two samples of similar characteristics with both faces in contact with the two samples surfaces. The measurements were performed with heating power ranging from 7 to 9 W and measurement time from 20 to 80 s. From the PF and κ values, ZT has been determined at room temperature and estimated at higher temperatures, together with its calculated error from the uncertainties of each physical parameter (S, ρ, and κ). For this estimation, the κ behaviour with temperature has been consulted in other works where it has been found to be nearly constant [28] or decreasing [29] when the temperature is increased. As a

consequence it has been assumed that, in the worst case, κ would be unchanged with T.

3. Results and discussion

3.1. As-grown samples

Powder XRD data for as-grown samples with different Pb content are plotted (from 10 to 40 ° for a better clarity) in Fig. 1. They show similar patterns where most of the peaks correspond to the (00l) planes of the misfit cobaltite $Bi_2Ba_2Co_2O_y$ [28]. Even if minor differences are found in weak peaks, the cobaltite phase appears as the major one, independently of the Pb content. Peak marked with a * in the plot corresponds to a Bi-Ba-O solid solution with P121/n1 space group [30]. Moreover, the proportion of the secondary phase is decreasing, compared to the thermoelectric one, when the Pb content in the samples is raised, as can be observed by the decrease of its (200) peak intensity.

Scanning electron microscopy was performed on longitudinal polished sections of the as-grown samples, and representative images of all samples are displayed in Fig. 2. In these images, three main contrasts can be seen (indicated by numbers in Fig. 2a for clarity). The major phase in all samples (grey contrast, #1) has been identified by EDS as the misfit thermoelectric $(Bi,Pb)_2Ba_2Co_2O_y$ one. In the case of the Pb-doped samples, this phase has a Pb content of around 0.4 for the 0.2Pb-doped one, slightly decreasing for higher Pb nominal composition. Dark grey contrast (#2) corresponds to the $Ba_2Co_3O_z$ secondary phase, while the white contrast (#3) has been identified as $Bi_5Ba_4O_x$, in agreement with the XRD data. Moreover, this last phase has an increasing Pb content with the nominal one, reaching a Bi:Ba:Pb proportion of 5:4:1 for the highest Pb nominal composition. This type of phases (plumbate-like ones) are well common in other Pb-doped systems [31] for their ability to admit very high Pb proportions, which can explain the slight decrease of Pb in the thermoelectric $(Bi,Pb)_2Ba_2Co_2O_y$ phase. Finally, in 0.6Pb-doped samples, a new contrast appears (black one, #4) which corresponds to Co-oxide. Other feature that can be observed in these microstructures is the decrease of $Ba_2Co_3O_z$ secondary phase when Pb content is raised while the thermoelectric one increases, in agreement with the XRD data. On the other hand, the plumbate-

like phase content seems to slightly increase with Pb-content. All these features are maintained until 0.4 Pb nominal content and further Pb substitution produces new phases (#4 in Fig. 2d) and clearly destroys the grain orientation in the bulk material. In any case, it can be easily seen that the best aligned grains are those found in samples with 0.2 Pb substitution.

The temperature dependence of the electrical resistivity, as a function of the Pb content, is given in Fig. 3. As it can be easily seen, $\rho(T)$ curves show a semiconducting-like behaviour ($d\rho/dT < 0$) in the whole temperature range. Moreover, the curve slope tends to be lower when Pb content is raised. This is in agreement with previous works which showed that Bi substitution by Pb increases the hole carrier concentration in similar systems [20,32]. This is due to the fact that Pb^{2+} is substituting Bi^{3+} in the RS structure leading to a decrease on the effective charge in this structure. As a consequence, the charge in the conducting layer has to be raised in order to compensate the changes in the RS layer, increasing the relative proportion of Co^{4+} in this layer. From Koshibae expression [33], the higher relationship between Co^{4+} and the total Co in the conducting layer (Co^{3+}+Co^{4+}) increases the carrier concentration, leading to lower electrical resistivity values at room temperature. On the other hand, the evolution of resistivity for the Pb doped samples clearly agree with the SEM and EDS data discussed previously. In fact, the lowest resistivity is measured on 0.2Pb doped samples due to their higher grain orientation (see Fig. 2) and to the fact that $Bi_2Ba_2Co_2O_y$ thermoelectric phase has the highest Pb content. Further Pb substitution produces higher grain misalignment and a slight decrease of Pb in the thermoelectric phase, leading to increased resistivity values compared to the 0.2Pb doped samples. The minimum resistivity value (~ 11 mΩ cm) at 650 ºC has been obtained for the 0.2Pb doped samples, which is slightly higher than the best results obtained in pure $Bi_2Ba_2Co_2O_y$ textured by the LFZ technique at low rates (~ 8.5 mΩ cm) [34], but much lower than the obtained in sintered materials (~ 33 mΩ cm) [28].

Fig. 4 displays the variation of Seebeck coefficient with temperature as a function of Pb content. As can be easily seen in the plot, S is positive in the whole measured temperature range, indicating a conduction mechanism mainly governed by holes. Moreover, all the samples show similar S values at room

temperature (~ 130 $\mu V\ K^{-1}$) which are slightly higher than the obtained in textured materials grown by the LFZ technique at low rates (~ 120 $\mu V\ K^{-1}$) [34], and much higher than the measured in sintered materials at the same temperature (~ 85 $\mu V\ K^{-1}$) [28]. On the other hand, different behaviours can be observed for the undoped and for the doped samples. The raise of S with temperature for the undoped samples is much lower than for the Pb doped ones. As a consequence, all the Pb doped samples reach higher S values at 650 ºC than the undoped ones. The highest S value at 650 ºC has been obtained for the 0.4Pb doped samples (~ 205 $\mu V\ K^{-1}$), which is around 35 % higher than the obtained in the undoped samples, and slightly higher (~ 5 %) than the measured in the other Pb doped ones. Moreover, this value is slightly higher than the obtained in textured materials grown by the LFZ technique at low rates (~ 185 $\mu V\ K^{-1}$) [34], and much higher than the measured in sintered materials at the same temperature (~ 110 $\mu V\ K^{-1}$) [28].

From the above data, PF has been calculated and presented, as a function of Pb content, in Fig. 5, where it can be clearly seen that the PF of the 0.2Pb doped samples raise, in a very important manner, with respect to the values obtained in undoped ones (~ 100 % in the whole measured temperature range). Further Pb doping starts to decrease PF values with respect to the 0.2Pb doped ones. This evolution is in clear agreement with the microstructural features discussed previously which showed that the best oriented grains and the highest amount of TE phase was obtained in the 0.2Pb doped samples. The highest PF values at room temperature and at 650 ºC (around 0.12 and 0.34 $mW\ K^{-2}\ m^{-1}$, respectively) are much higher than the obtained in solid state sintered materials (~ 0.035 and 0.040 $mW\ K^{-2}\ m^{-1}$, respectively) [28]. Moreover, they are also higher than the obtained at different growth rates. On the other hand, they are very close to the values obtained in pure $Bi_2Ba_2Co_2O_y$ materials textured at low rates (about 0.40 $mW\ K^{-2}\ m^{-1}$ at 650 ºC) [34].

It is important to highlight that all the above described results are around the best ones obtained in $Bi_2Ba_2Co_2O_y$ materials. Taking into account that the amount of secondary phases in the studied samples is relatively high, an annealing process could promote the formation of a higher proportion of TE phase. Consequently, this thermal treatment would decrease the amount of

secondary phases leading, at least, to a lower electrical resistivity. In order to determine the adequate annealing temperature, DTA analysis has been performed on the as-grown samples (diagrams not shown). All the curves showed a continuous endothermic behaviour in the high temperature range. As a consequence, the best annealing temperature for the thermal treatment of as-grown samples has been experimentally found to be 700 ºC.

3.2. Annealed samples

After annealing at 700 ºC for 24 h with a final cooling inside the furnace, powdered samples were characterized by XRD, and the results are plotted in Fig. 6. As can be observed in the plot, all the samples exhibit patterns similar (to the as-grown ones, where most of the peaks correspond to the (00l) planes of the misfit cobaltite $Bi_2Ba_2Co_2O_y$ [28] which is the major one, independently of Pb content. The peak marked with a * in the plot corresponds to a Bi-Ba-O solid solution with P121/n1 space group [30], which is decreasing in intensity, compared to the thermoelectric one, when the Pb content in the samples is raised. Moreover, the intensity of this (002) peak is clearly smaller than the one obtained in as-grown samples, indicating a decrease of secondary phase content with the thermal treatment.

Scanning electron microscopy performed on longitudinal polished sections of annealed samples has confirmed the evolution described in the XRD discussion, as can be observed in the representative images displayed in Fig. 7. In the pictures, three main contrasts can be observed (indicated by numbers in Fig. 7a for clarity). The major phase in all samples (grey contrast, #1) has been identified by EDS as the misfit thermoelectric $(Bi,Pb)_2Ba_2Co_2O_y$ one. In the case of the Pb-doped samples, this phase has a Pb content of around 0.4 in all cases. Dark grey contrast (#2) corresponds to the $Ba_2Co_5O_z$ secondary phase which possesses higher Co content than in the as-grown samples, while the white contrast (#3) has been identified as $Bi_2Ba_4O_x$ with lower Bi content than in the as-grown ones. Moreover, this last phase has an increasing Pb content with the nominal one, reaching a Bi:Ba:Pb proportion of 2:4:1 for the highest Pb nominal composition. In any case, the amount of this plumbate-like phase is very low in the case of 0.2 and 0.4 Pb doped samples due to the Pb incorporation in the thermoelectric phase (which is around 0.4Pb in all cases).

The temperature dependence of the electrical resistivity as a function of Pb content for the annealed samples is shown in Fig. 8. As it can be easily seen, Pb addition clearly decreases the electrical resistivity values in the whole measured temperature range, in agreement with previous reports [35]. Moreover, the $\rho(T)$ curves show nearly a metallic-like behaviour ($d\rho/dT > 0$) in the whole studied temperature range. This behaviour is totally different to the one observed in the as-grown samples (see Fig. 3) and can be associated to the higher amount of thermoelectric phase in the annealed ones, together with a higher oxygen content. This is in agreement with previous works which showed that LFZ processing of these materials generates oxygen vacancies in larger content than in bulk samples synthesized by a classic solid-state reaction [17]. As a consequence, the annealing process can lead to an increase of oxygen in the structure, in agreement with the decrease of electrical resistivity in the annealed samples, compared with the as-grown ones (see Figs. 3 and 8). The lowest resistivity value at 650 ºC has been obtained in the 0.2 Pb doped annealed samples (~ 6 mΩ cm) which is nearly half of the obtained in the as-grown ones (around 11 mΩ cm). Moreover, it is much smaller than the measured in sintered materials (about 33 mΩ cm) [28], in $Bi_{1.8}Pb_{0.2}Ba_2Co_2O_y$ materials annealed under 0.1% O_2 atmosphere (around 70 mΩ cm) [36], or in highly textured materials grown by LFZ at low rates (~ 8.5 mΩ cm) [34].

Fig. 9 displays the variation of the Seebeck coefficient as a function of temperature for all the annealed samples. As it can be observed, all samples possess, approximately, the same S values in the whole measured temperature range. At first sight, the most remarkable difference can be found in the drastic change in Seebeck coefficient between as-grown and annealed undoped samples. This effect can be due to the fact that Pb^{2+} substitution for Bi^{3+} should lead to a decrease of the total oxygen content in the thermoelectric phase, leading to a lower effect of the LFZ processing on the oxygen vacancies. This explanation is in agreement with the small changes in the Seebeck coefficient between as-grown and annealed Pb doped samples (see Figs. 4 and 9). Moreover, the Seebeck coefficient values at room temperature for the annealed samples (around 115 $\mu V\ K^{-1}$) are lower than the obtained in as-grown ones (about 130 $\mu V\ K^{-1}$) which clearly agree with the increase in oxygen in the

structure produced by the annealing process discussed previously. In any case, the highest S value at 650 ºC has been obtained for the undoped samples (~ 185 $\mu V\ K^{-1}$) which is the same value obtained in textured materials grown by the LFZ technique at low rates (~ 185 $\mu V\ K^{-1}$) [34], and much higher than the measured in sintered materials at the same temperature (~ 110 $\mu V\ K^{-1}$) [28], or in $Bi_{1.8}Pb_{0.2}Ba_2Co_2O_y$ materials annealed under 0.1 % O_2 atmosphere (around 120 $\mu V\ K^{-1}$) [36].

From the electrical resistivity and Seebeck coefficient data, PF has been calculated and represented, as a function of temperature, in Fig. 10. As it can be observed in the graph, the drastic decrease of electrical resistivity of annealed samples with only a slight decrease of Seebeck coefficient, leads to a higher PF values than the ones obtained in as-grown samples. At room temperature, annealed samples show PF values about two times higher in all cases. Moreover, the maximum PF value at 650 ºC (about 0.45 mW K^{-2} m^{-1}) for the 0.2 Pb doped samples is 30 % higher than the best value obtained in the best as-grown ones (see Fig. 5). More interesting, this value is much higher than the one obtained in solid state sintered materials (~ 0.040 mW K^{-2} m^{-1}) [28] or in $Bi_{1.8}Pb_{0.2}Ba_2Co_2O_y$ materials annealed under 0.1 % O_2 atmosphere (around 0.030 mW K^{-2} m^{-1}) [36] and slightly higher than those measured in pure $Bi_2Ba_2Co_2O_y$ materials textured at low rates (about 0.40 mW K^{-2} m^{-1}) [34] at the same temperature.

Thermal conductivity values at room temperature in all the textured-annealed samples were 0.493, 0.561, 0.505, and 0.623 W K^{-1} m^{-1} for the 0.0, 0.2, 0.4, and 0.6 Pb-doped samples, respectively. On the other hand, as it is well known, the thermal conductivity can be expressed by a sum of lattice component (κ_l) and electronic component (κ_e), $\kappa = \kappa_l + \kappa_e$, and $\kappa_e = L\sigma T$, where L is Lorenz number, σ electrical conductivity, and T absolute temperature. As Pb substitution increases the electrical conductivity, compared with the undoped samples, κ_e of Pb-doped samples is expected to be larger than that of Pb-free ones, explaining the higher thermal conductivity of Pb-doped samples. In any case, the measured values are much lower than the obtained in the $Bi_2Ba_2Co_2O_y$ sintered materials (~ 1 W K^{-1} m^{-1} at room temperature) [28], or in $Bi_{1.8}Pb_{0.2}Ba_2Co_2O_y$

materials annealed under 0.1% O_2 atmosphere (~ 1 W K^{-1} m^{-1} at room temperature) [36].

With PF and κ data, ZT has been calculated at room temperature, which showed the values 0.014, 0.031, 0.028, and 0.019 for the 0.0, 0.2, 0.4, and 0.6 Pb-doped samples, respectively. These values are very small for practical applications, but it should be considered that thermoelectric oxides are adequate for high temperature devices. Moreover, when compared with the reported values in the literature at this temperature (0.0021, and 0.0075 for 0.0, and 0.2 Pb-doped samples, respectively [36]), the values achieved in this work are more than four times higher than the previously presented. Moreover, with the approximation of κ constant with temperature, estimated ZT values at 650 ºC would be 0.38, 0.53, 0.52, and 0.34 for the 0.0, 0.2, 0.4, and 0.6 Pb-doped samples, respectively. Taking into account this consideration, estimated ZT values are presented in Fig. 11. As it can be observed, 0.2 and 0.4 Pb-doped samples possess very similar ZT values, clearly higher than the undoped ones while the 0.6 Pb-doped ones show the lowest values. The maximum ZT value obtained in these samples, 0.53 for the 0.2 Pb-doped ones is about two times higher than the obtained in solid state sintered $Bi_2Ba_2Co_2O_y$ materials (~ 0.25) [28]. Moreover, all the textured-annealed samples prepared in this work show higher ZT than these sintered materials. It is clear that this calculated value has an uncertainty is determined by the individual physical parameters uncertainties used to get the ZT result, specifically electrical resistivity, Seebeck coefficient and thermal conductivity. This way, the relative error of ZT was determined by the principle of error propagation. Moreover, taking into account the number of measurements performed at each temperature, the value of error corresponds to the upper limit of the error. Using this procedure, it is possible to forecast the maximum uncertainty associated to the determined value. The electrical resistivity error estimation obtained was 4 % taking into account the sensitivity of the measuring apparatus and the inaccuracy in measuring the dimensions of the samples and the distance between the contacts. An error of around 4% was also estimated for Seebeck coefficient, which is also influenced by the error of the thermocouples in determining the temperature difference of the cold and hot sides of the sample. For the error in the thermal conductivity (k) better accuracy

than 5% is stated by the equipment manufacture. Hence, considering all these values together in the mathematical formula of error propagation a maximum 16 % error for ZT was estimated. It is important to highlight that this error value is in accordance to the international analysis of ZT measurements that have conclude that the uncertainty in ZT values is around 15 % [37,38].

Noteworthy, all these results indicate that textured and annealed $Bi_{1.8}Pb_{0.2}Ba_2Co_2O_y$ materials are good bulk ceramic candidates for applications in thermoelectric generators.

4. Conclusions

Textured Pb doped $Bi_{2-x}Pb_xBa_2Co_2O_y$ materials, with x= 0, 0.2, 0.4, and 0.6 were successfully prepared by the laser floating zone method. XRD and SEM characterization have shown that as-grown materials are mainly composed of the thermoelectric $(Bi,Pb)_2Ba_2Co_2O_y$ phase accompanied of several secondary phases. The amount of these secondary phases decreases with Pb addition until 0.4Pb, increasing the proportion of thermoelectric phase. Further decrease of the amount of secondary phases has been performed by annealing at 700 ºC, leading to higher thermoelectric performance than the measured in the as-grown samples. The best PF values obtained at 650 ºC for the 0.2 Pb doped samples is the highest reported in the best of our knowledge, around 10 times higher than the obtained in solid state sintered materials and about 10 % higher than the measured in pure laser grown $Bi_2Ba_2Co_2O_y$ materials at low rates. The low thermal conductivity of the textured annealed samples leads to a maximum estimated ZT value of 0.53 for the 0.2 Pb-doped samples, which is about two times higher than the obtained in solid state sintered undoped ones reported in the literature. This raise in ZT is very important even if the real value could be decreased by a maximum of 16 % due to the measurements error.

5. Acknowledgements

This research has been supported by the Spanish MINECO-FEDER (MAT2013-46505-C3-1-R). The authors wish to thank the Gobierno de Aragón-Fondo Social Europeo (Consolidated Research Groups T12 and T87) for financial support and to C. Gallego, C. Estepa and J. A. Gomez for their technical assistance. The authors also acknowledge the PEst-C/CTM/LA 25/2013-14,

RECI/CTM-CER/0336/2012 co-financed by FEDER, QREN reference COMPETE: FCOMP-01-0124-FEDER-027465, “Facing the challenges of characterizing novel thermal materials and processes (Heat@UA)” and CICECO-Aveiro Institute of Materials (Ref. FCT UID /CTM /50011/2013) funding.

References

[1] Biswas K, He J, Blum ID, Wu C-I, Hogan TP, Seidman DN, Dravid VP, Kanatzidis MG. High-performance bulk thermoelectrics with all-scale hierarchical architectures. Nature 2012;489:414–8.

[2] Liu W, Yan X, Chen G, Ren Z. Recent advances in thermoelectric nanocomposites. Nano Energy 2012;1:42–56.

[3] Elsheikh MH, Shnawah DA, Sabri MFM, Said SBM, Hassan MH, Bashir MBA, Mohamad M. Renew Sust Energ Rev 2014;30:337–55.

[4] Rowe DM. Thermoelectrics Handbook: Macro to Nano. first ed. Boca Raton:CRC Press;2006.

[5] Terasaki I, Sasago Y, Uchinokura K. Large thermoelectric power in NaCo2O4 single crystals. Phys Rev B 1997;56 (20):12685–7.

[6] Sotelo A, Rasekh Sh, Madre MA, Guilmeau E, Marinel S, Diez JC. Solution-based synthesis routes to thermoelectric $Bi_2Ca_2Co_{1.7}O_x$. J Eur Ceram Soc 2011;31:1763–9.

[7] Sun N, Dong ST, Zhang BB, Chen YB, Zhou J, Zhang ST, Gu ZB, Yao SH. Chen YF. Intrinsically modified thermoelectric performance of alkaline-earth isovalently substituted $[Bi_2AE_2O_4][CoO_2]_y$ single crystals. J Appl Phys 2013;114:043705.

[8] Rubesova K, Hlasek T, Jakes V, Huber S, Hejtmanek J, Sedmidubsky D. Effect of a powder compaction process on the thermoelectric properties of Bi2Sr2Co1.8Ox ceramics. J Eur Ceram Soc 2015;35:525–31.

[9] Diez JC, Guilmeau E, Madre MA, Marinel S, Lemmonier S, Sotelo A, Improvement of $Bi_2Sr_2Co_{1.8}O_x$ thermoelectric properties by laser floating zone texturing. Solid State Ionics 2009;180:827–30.

[10] Hervieu M, Maignan A, Michel C, Hardy V, Creon N, Raveau B. Metallicity and thermopower of the misfit cobaltite $[Bi_2Ba_{1.8}Co_{0.2}O_4]^{RS}[CoO_2]_2$. Phys Rev B 2003;67:045112.

[11] Wu N, Holgate TC, Nong NV, Pryds N, Linderoth S. High temperature thermoelectric properties of $Ca_3Co_4O_{9+\delta}$ by auto-combustion synthesis and spark plasma sintering. J Eur Ceram Soc 2014;34:925–31.

[12] Sotelo A, Constantinescu G, Rasekh Sh, Torres MA, Diez JC, Madre MA. Improvement of thermoelectric properties of $Ca_3Co_4O_9$ using soft chemistry synthetic methods. J Eur Ceram Soc 2012;32:2415–22.

[13] Leligny H, Grebille D, Perez O, Masset AC, Hervieu M, Raveau R. A five-dimensional structural investigation of the misfit layer compound $[Bi_{0.87}SrO_2]_2[CoO_2]_{1.82}$. Acta Cryst *B* 2000;56:173–82.

[14] Maignan A, Hébert S, Hervieu M, Michel C, Pelloquin D, Khomskii D, Magnetoresistance and magnetothermopower properties of Bi/Ca/Co/O and Bi(Pb)/Ca/Co/O misfit layer cobaltites. J Phys: Condens Matter 2003;15:2711–23.

[15] Wang H, Sun X, Yan X, Huo D, Li X, Li JG, Ding X. Fabrication and thermoelectric properties of highly textured $Ca_9Co_{12}O_{28}$ ceramic. J Alloys Compds 2014;582:294–8.

[16] Butt S, Liu YC, Lan JL, Shehzad K, Zhan B, Lin Y, Nan CW. High-temperature thermoelectric properties of La and Fe co-doped Ca–Co–O misfit-layered cobaltites consolidated by spark plasma sintering. J Alloys Compds 2014;588:277–83.

[17] Diez JC, Rasekh Sh, Madre MA., Guilmeau E, Marinel S, Sotelo A. Improved Thermoelectric Properties of Bi-M-Co-O (M = Sr, Ca) Misfit Compounds by Laser Directional Solidification. J Electron Mater 2010;39:1601–5.

[18] Ferreira NM, Rasekh Sh, Costa FM, Madre MA, Sotelo A, Diez JC,Torres M.A. New method to improve the grain alignment and performance of thermoelectric ceramics. Mater Lett 2012;83:144–7.

[19] Abdellahi M, Bahmanpour M, Bahmanpour M. Modeling Seebeck coefficient of $Ca_{3-x}M_xCo_4O_9$ (M=Sr, Pr, Ga, Ca, Ba, La, Ag) thermoelectric ceramics. Ceram Int 2015;41:345–52.

[20] Sotelo A, Rasekh Sh, Guilmeau E, Madre MA, Torres MA, Marinel S, Diez JC, Improved thermoelectric properties in directionally grown $Bi_2Sr_2Co_{1.8}O_y$ ceramics by Pb for Bi substitution. Mater Res Bull 2011;46:2537–42.

[21] Rasekh Sh, Madre MA, Sotelo A, Guilmeau E, Marinel S, Diez JC. Effect of synthetic methods on the thermoelectrical propertiesof textured $Bi_2Ca_2Co_{1.7}O_x$ ceramics. Bol Soc Esp Ceram V 2010;49:89–94.

[22] Xie R, Liu C, Zhao Y, Jin P, Zhou KC, Zhang D. Gelation behavior and mechanical properties of gelcast lead zirconatetitanate ceramics. J Eur Ceram Soc 2015;35:2051–6.

[23] Sotelo A, de La Fuente GF, Lera F, Beltran D, Sapina F, Ibanez R, Beltran A, Bermejo MR. Novel Polymer Solution Synthesis of the 110 K Superconducting Phase in the Bismuth. System Chem Mater 1993;5:851–6.
[24] Madre MA, Rasekh Sh, Diez JC, Sotelo A. New solution method to produce high performance thermoelectric ceramics: A case study of Bi-Sr-Co-O. Mater Lett 2010;64:2566–8.
[25] Rasekh Sh, Constantinescu G, Torres MA, Madre MA, Diez JC, Sotelo A. Growth rate effect on microstructure and thermoelectric properties of melt grown $Bi_2Ba_2Co_2O_x$ textured ceramics. Adv Appl Ceram 2012;111:490–4.
[26] Sotelo A, Guilmeau E, Madre MA, Marinel S, Lemmonier S, Diez JC. $Bi_2Ca_2Co_{1.7}O_x$ thermoelectric ceramics textured by laser floating zone method Bol Soc Esp Ceram V 2008;47:225–8.
[27] de la Fuente GF, Ruiz MT, Sotelo A, Larrea A, Navarro R.Microstructure of laser floating zone (LFZ) textured (Bi,Pb)-Sr-Ca-Cu-O superconductor composite. Mater Sci Eng A 1993;173:201–4.
[28] Hao H, Yang H, Liu Y, Hu X. High-temperature Thermoelectric Properties of Cu-substituted $Bi_2Ba_2Co_{2-x}Cu_xO_y$ Oxides. J Mater Sci Technol 2011;27:525–8.
[29] He QL, Qin Z, Zhang J, Gao F, Hu X, Song HZ. Enhanced Thermoelectric Properties of Hole-Doped $Bi_{2-x}Ba_xSr_2Co_2O_y$ Ceramics. J Electron Mater 2014;43:1432–5.
[30] Kennedy BJ, Howard CJ, Knight KS, Zhang ZM, Zhou QD. Structures and phase transitions in the ordered double perovskites $Ba_2Bi^{III}Bi^{V}O_6$ and $Ba_2Bi^{III}Sb^{V}O_6$. Acta Cryst B 2006;62:537–46.
[31] Madre MA, Amaveda H, Mora M, Sotelo A, Angurel LA, Diez JC. Ag doped $(Bi_{1.6}Pb_{0.4})Sr_2CaCu_2O_{8+\delta}$ textured rods. Bol Soc Esp Ceram V 2008;47:148–52.
[32] Rasekh Sh, Madre MA, Diez JC, Guilmeau E, Marinel S, Sotelo, A. Effect of Pb substitution on the thermoelectrical properties of textured $Bi_2Ca_2Co_{1.7}O_y$ ceramics prepared by a polymer solution method. Bol Soc Esp Ceram V 2010;49:371–6.
[33] Koshibae W, Tsuitsui K, Maekawa S. Thermopower in cobalt oxides. Phys Rev B 2000;62:6869–72.

[34] Constantinescu G, Rasekh Sh, Torres MA, Madre MA, Diez JC, Sotelo A. Enhancement of the high-temperature thermoelectric performance of $Bi_2Ba_2Co_2O_x$ ceramics. Scr Mater 2013;68:75–8.

[35] Kobayashi W, Muguerra H, Hebert S, Grebille D, Maignan A. Metallicity and positive magnetoresistance induced by Pb substitution in a misfit cobaltate crystal. J. Phys.: Cond. Matter 2009;21:235404.

[36] Sakai K, Karppinen M, Chen JM, Liu RS, Sugihara S, Yamauchi H. Pb-for-Bi substitution for enhancing thermoelectric characteristics of $[(Bi,Pb)_2Ba_2O_{4\pm\omega}]_{0.5}CoO_2$. Appl Phys Lett 2006;88:232102.

[37] Populoh S, Aguirre MH, Brunko OC, Galazka K, Lu Y, Weidenkaff A. High figure of merit in (Ti,Zr,Hf)NiSn half-Heusler alloys. Scr. Mater. 2012;66:1073–1076.

[38] Thiel P, Populoh S, Yoon S, Weidenkaff A. Enhancement of redox– and phase-stability of thermoelectric $CaMnO_{3+\delta}$ by substitution. J. Solid State Chem. 2015;229:62–67.

Figure captions

Figure 1. Powder XRD plots of the $Bi_{2-x}Pb_xBa_2Co_2O_x$ as-grown samples with different Pb contents. x = 0.0 (a), 0.2 (b), 0.4 (c), and 0.6 (d). Diffraction planes indicates the $Bi_2Ba_2Co_2O_x$ phase while * shows the peak corresponding to the $BiBaO_3$ secondary phase.

Figure 2. Scanning electron micrographs obtained on transversal polished sections of $Bi_{2-x}Pb_xBa_2Co_2O_x$ as-grown samples with x= 0.0 (a), 0.2 (b), 0.4 (c), and 0.6 (d). Different contrasts are #1: grey one, associated to the thermoelectric $(Bi,Pb)_2Ba_2Co_2O_x$ phase; #2: dark grey, $Ba_2Co_3O_y$; #3: white, $Bi_5Ba_4O_z$ with plumbate-like composition (around $Bi_5Ba_4PbO_z$) in the Pb-substituted samples; and #4: black, Co-oxide.

Figure 3. Temperature dependence of the electrical resistivity for the as-grown $Bi_{2-x}Pb_xBa_2Co_2O_x$ samples, for x= 0.0 ■; 0.2 ● 0.4 ▲; and 0.6 ▼.

Figure 4. Temperature dependence of the Seebeck coefficient for the as-grown $Bi_{2-x}Pb_xBa_2Co_2O_x$ samples, for x= 0.0 ■; 0.2 ● 0.4 ▲; and 0.6 ▼.

Figure 5. Temperature dependence of power factor for the as-grown $Bi_{2-x}Pb_xBa_2Co_2O_x$ samples, for x= 0.0 ■; 0.2 ● 0.4 ▲; and 0.6 ▼.

Figure 6. Powder XRD plots of the $Bi_{2-x}Pb_xBa_2Co_2O_x$ as-grown samples with different Pb contents. x = 0.0 (a), 0.2 (b), 0.4 (c), and 0.6 (d). Diffraction planes indicates the $Bi_2Ba_2Co_2O_x$ phase while * shows the peak corresponding to the $BiBaO_3$ secondary one.

Figure 7. Scanning electron micrographs obtained on transversal polished sections of $Bi_{2-x}Pb_xBa_2Co_2O_x$ annealed samples with x= 0.0 (a), 0.2 (b), 0.4 (c), and 0.6 (d). Different contrasts are #1: grey one, associated to the thermoelectric $(Bi,Pb)_2Ba_2Co_2O_x$ phase; #2: dark grey, $Ba_2Co_5O_y$; #3: white, and $Bi_2Ba_4O_z$ with plumbate-like composition (around $Bi_2Ba_4PbO_z$) in the Pb-substituted samples.

Figure 8. Temperature dependence of the electrical resistivity for the annealed $Bi_{2-x}Pb_xBa_2Co_2O_x$ samples, for x= 0.0 ■; 0.2 ● 0.4 ▲; and 0.6 ▼.

Figure 9. Temperature dependence of the Seebeck coefficient for the annealed $Bi_{2-x}Pb_xBa_2Co_2O_x$ samples, for x= 0.0 ■; 0.2 ● 0.4 ▲; and 0.6 ▼.

Figure 10. Temperature dependence of power factor for the annealed $Bi_{2-x}Pb_xBa_2Co_2O_x$ samples, for x= 0.0 ■; 0.2 ● 0.4 ▲; and 0.6 ▼.

Figure 11. Estimated temperature dependence of ZT for the annealed $Bi_{2-x}Pb_xBa_2Co_2O_x$ samples, for x= 0.0 ■; 0.2 ● 0.4 ▲; and 0.6 ▼.

Figure 1

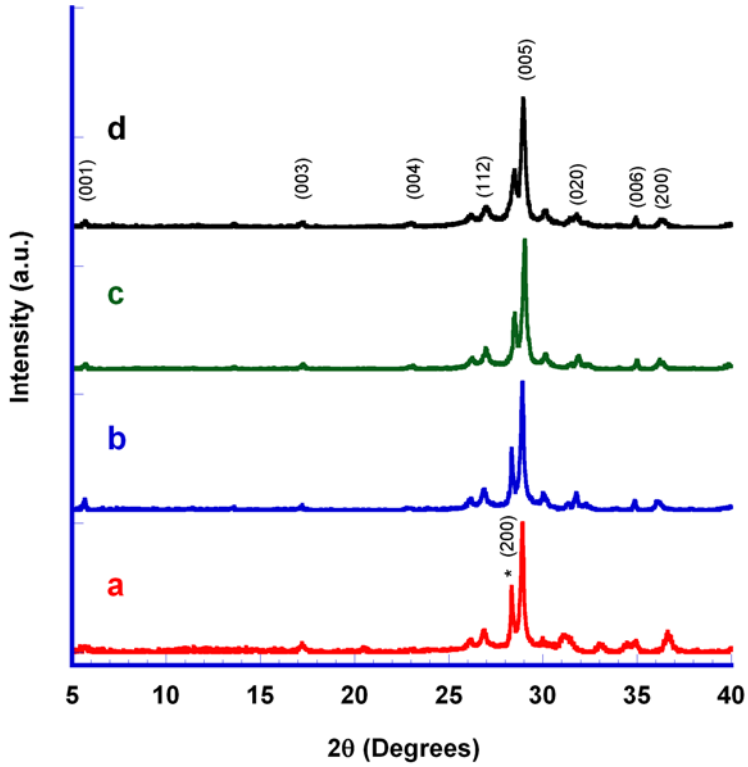
d
c
b
a
(001)
(003)
(004)
(112)
(005)
(020)
(006)
(200)
(200)
*
Intensity (a.u.)
5
10
15
20
25
30
35
40
2θ (Degrees)

Figure 2

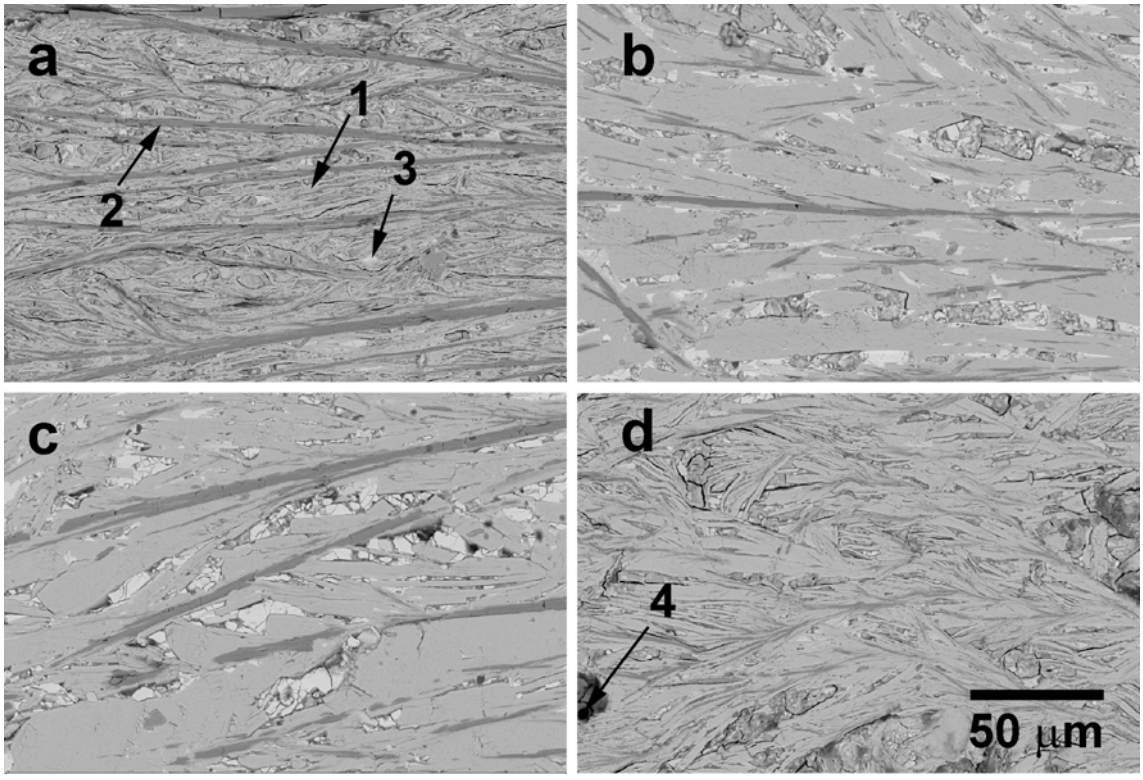

Figure 3

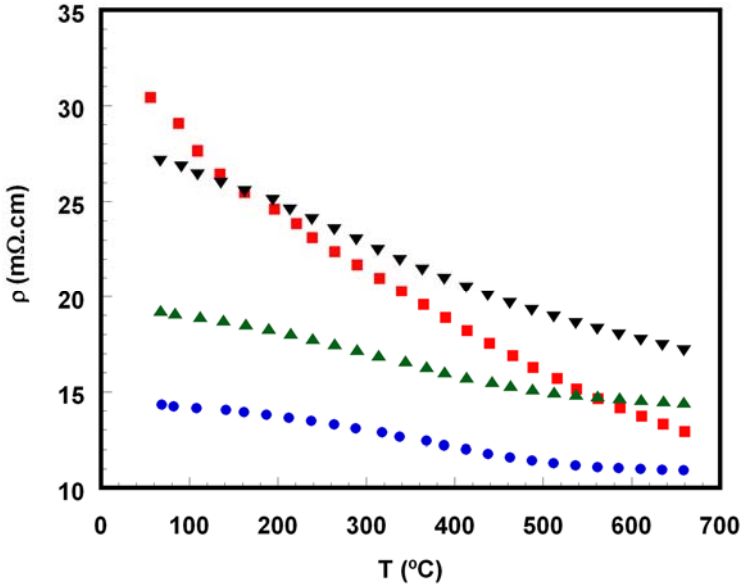

Figure 4

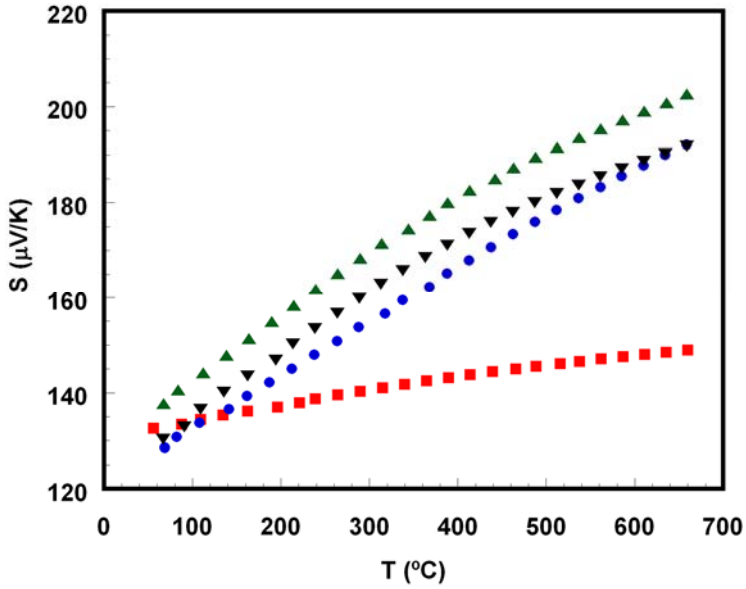

Figure 5

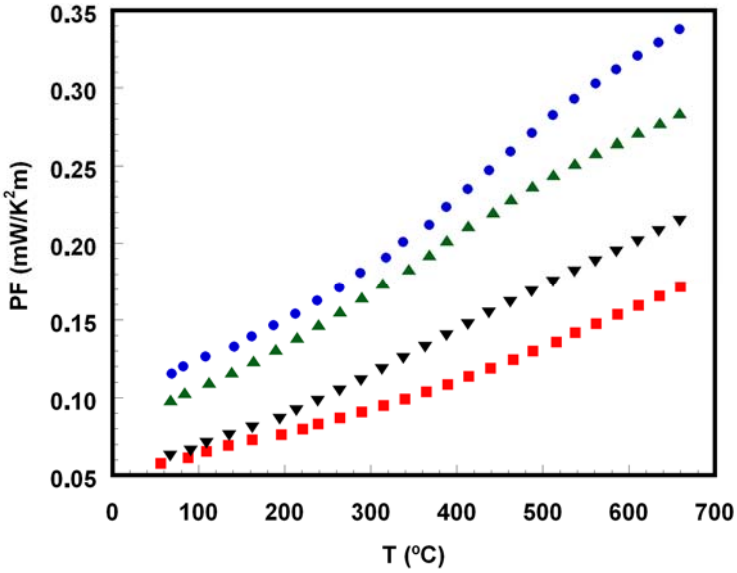
0.35
0.30
0.25
0.20
0.15
0.10
0.05
PF (mW/K²m)
0
100
200
300
400
500
600
700
T (°C)

Figure 6

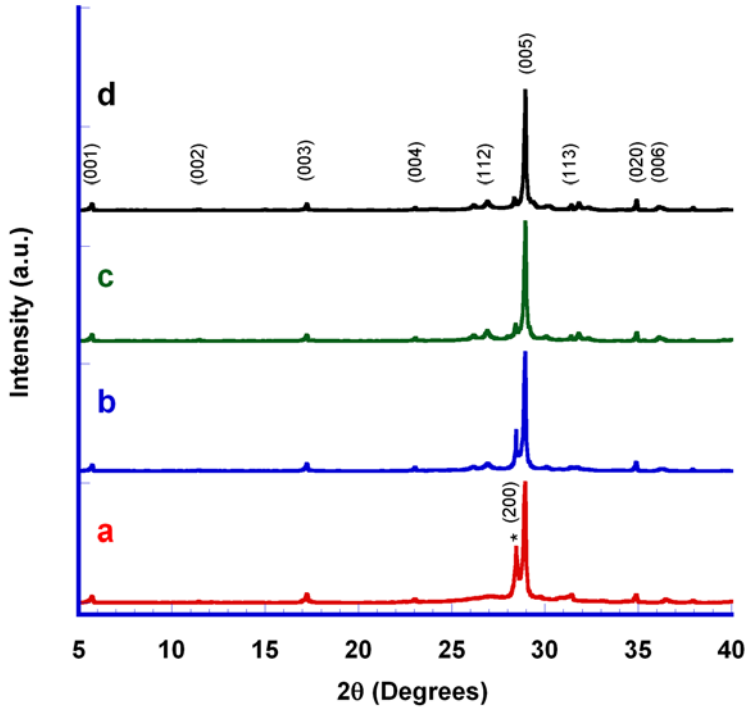
d
c
b
a
(001)
(002)
(003)
(004)
(112)
(005)
(113)
(020)
(006)
(200)
*
Intensity (a.u.)
5
10
15
20
25
30
35
40
2θ (Degrees)

Figure 7

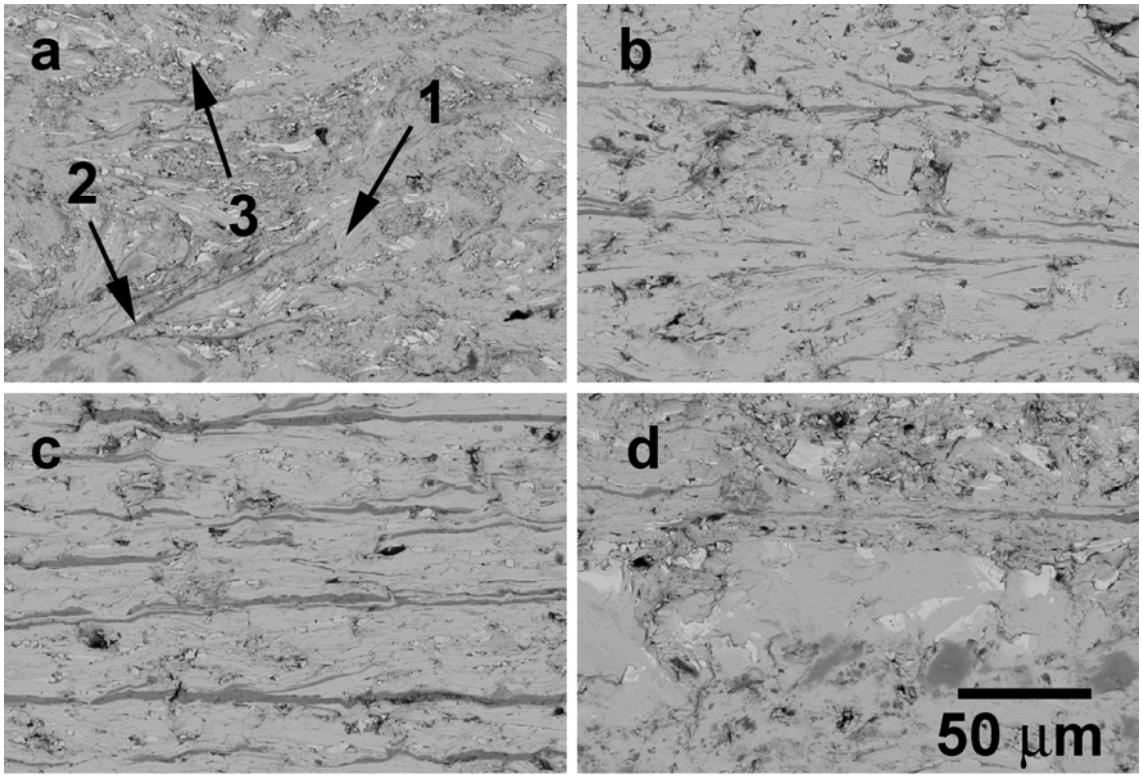

Figure 8

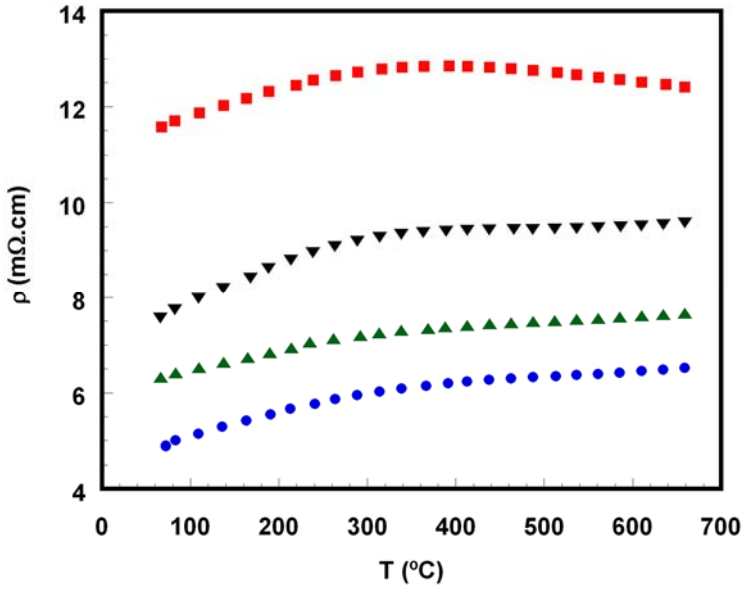

Figure 9

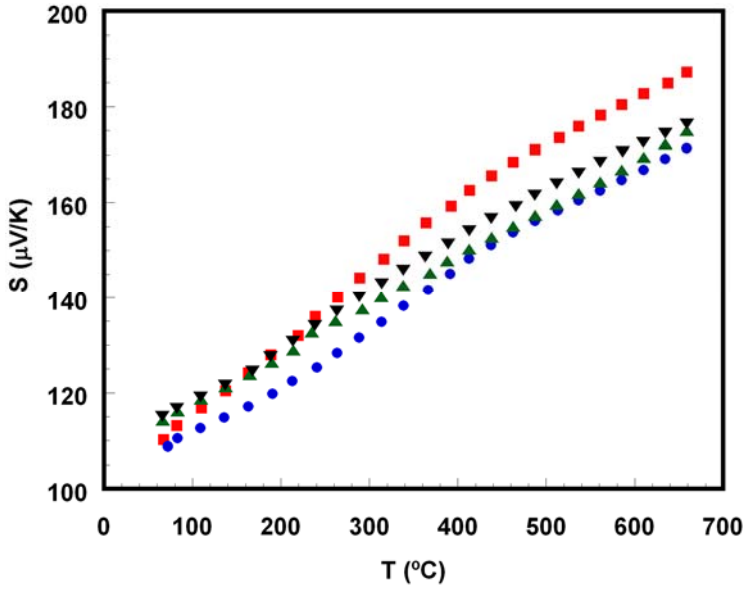

Figure 10

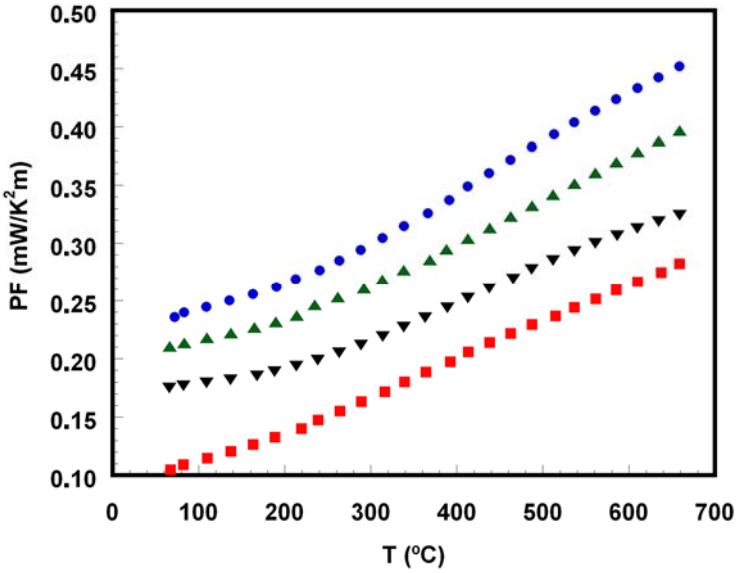
0.50
0.45
0.40
0.35
0.30
0.25
0.20
0.15
0.10
PF (mW/K²m)
0
100
200
300
400
500
600
700
T (°C)

Figure 11